The physical basis for increases in precipitation extremes in simulations of 21st-century climate change

Paul A. O'Gorman[a,1] and Tapio Schneider[b]

[a]Massachusetts Institute of Technology, Cambridge, MA 02139; and [b]California Institute of Technology, Pasadena, CA 91125

Communicated by Kerry A. Emanuel, Massachusetts Institute of Technology, Cambridge, MA, July 14, 2009 (received for review March 24, 2009)

Global warming is expected to lead to a large increase in atmospheric water vapor content and to changes in the hydrological cycle, which include an intensification of precipitation extremes. The intensity of precipitation extremes is widely held to increase proportionately to the increase in atmospheric water vapor content. Here, we show that this is not the case in 21st-century climate change scenarios simulated with climate models. In the tropics, precipitation extremes are not simulated reliably and do not change consistently among climate models; in the extratropics, they consistently increase more slowly than atmospheric water vapor content. We give a physical basis for how precipitation extremes change with climate and show that their changes depend on changes in the moist-adiabatic temperature lapse rate, in the upward velocity, and in the temperature when precipitation extremes occur. For the tropics, the theory suggests that improving the simulation of upward velocities in climate models is essential for improving predictions of precipitation extremes; for the extratropics, agreement with theory and the consistency among climate models increase confidence in the robustness of predictions of precipitation extremes under climate change.

global warming | hydrological cycle | rainfall | extreme events

In simulations of 21st century climate change scenarios, mean precipitation generally increases in the deep tropics and extratropics and decreases in the subtropics (1–3). However, precipitation extremes (defined, for example, as a high percentile of daily precipitation) increase almost across the globe (2, 3), with expected societal impacts such as increased flooding and soil erosion (4). Precipitation extremes are widely held to increase proportionately to the mean atmospheric water vapor content (5, 6), or to the amount of water vapor converging at the base of storms (7). Global-mean water vapor content increases strongly in global warming simulations, at a rate of $\sim$7.5% K^{-1} with respect to surface temperature, approximately consistent with a constant effective relative humidity (1). Precipitation extremes are thought to increase at a similar rate, or maybe even more rapidly if the strength of the updrafts associated with extreme precipitation events increases as the climate warms (5, 6).

However, although precipitation extremes in simulations increase as the climate warms, their rate of increase varies with latitude and is generally not equal to the rate of increase in atmospheric water vapor content (6). Simulations of a wide range of climates with an idealized general circulation model show that precipitation extremes outside the subtropics scale more similarly to mean precipitation than to water vapor content (8). In simulations with comprehensive climate models, the rate of increase in precipitation extremes varies widely among models, particularly in the tropics (2). The variations among models in the tropics indicate that simulated precipitation extremes may depend sensitively on the parameterization of unresolved and poorly understood processes such as moist convection (9). Indeed, climate models do not correctly reproduce the interannual variability of precipitation extremes in the tropics (10), or the frequency and intensity distribution of precipitation generally (9, 11, 12).

It is difficult to use the relatively short observational record to quantify long-term global trends in precipitation extremes (13–15). Observations of interannual variability indicate that tropical precipitation extremes exhibit a greater sensitivity to temperature change than they would if they scaled with atmospheric water vapor content (10). However, the response of tropical precipitation extremes to warm anomalies (e.g., related to El Niño events) may differ from the response to global warming, for which the static stability changes throughout the tropics. Given the uncertainties in changes in precipitation extremes in simulations, and the difficulties in constraining these changes with observations, it is essential to assess more broadly how precipitation extremes change with climate in simulations and to provide a quantitative physical basis for understanding these changes.

Here, we assess how precipitation extremes change in simulations with 11 different climate models in the World Climate Research Program's (WCRP's) Coupled Model Intercomparison Project phase 3 (CMIP3) archive. We compare the 99.9th percentile of daily precipitation within model grid boxes for 20-year periods at the end of the 20th and 21st century, under a moderate scenario for greenhouse gas emissions (SRES A1B). The 99.9th percentile corresponds to the amount of daily precipitation exceeded with probability 1/1,000. We evaluate the changes in precipitation extremes as a function of latitude, aggregating daily grid-box precipitation amounts for all times and longitudes at a given latitude and computing 99.9th percentiles from their aggregate distribution. Similar results are obtained for changes in precipitation extremes when the percentiles are calculated at each grid box and their change is zonally averaged (6). Excluding dry days from the analysis also does not qualitatively change the results because we consider high percentiles that are not strongly affected by the low percentiles, and there are relatively few dry days in the climate model simulations. Changes in precipitation extremes with climate may differ for hourly and daily accumulations (16); we consider precipitation accumulated over a day because precipitation on shorter time scales may not be well resolved in climate models and is not typically archived, and because accumulations over a day or longer are relevant for flooding (17, 18).

Results

The 99.9th percentile of daily precipitation is comparable in magnitude in the 20th-century multimodel median of the simulations and in observations from the Global Precipitation

Author contributions: P.A.O. and T.S. designed research; P.A.O. and T.S. performed research; P.A.O. analyzed data; and P.A.O. and T.S. wrote the paper.

The authors declare no conflict of interest.

[1]To whom correspondence should be addressed. E-mail: pog@mit.edu.

This article contains supporting information online at www.pnas.org/cgi/content/full/0907610106/DCSupplemental.

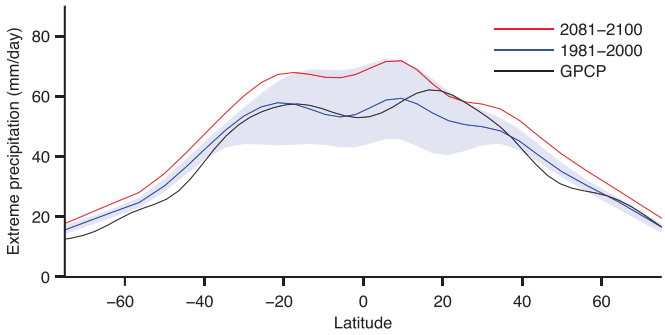

Fig. 1. The 99.9th percentile of daily precipitation (millimeters per day) for the periods 1981–2000 (blue) and 2081–2100 (red) in the SRES A1B scenario (multimodel median), and based on Global Precipitation Climatology Project (GPCP) data for the period 1997–2006 (black). Model scatter (shading) for the period 1981–2000 is shown using the interquartile range (50% of models lie within the shaded region). The spatial resolution of the GPCP data were degraded from 1° to 3°, which is comparable with climate model resolutions. A Gaussian smoothing filter of standard deviation 6° latitude was applied to reduce noise in all plots showing variations with latitude.

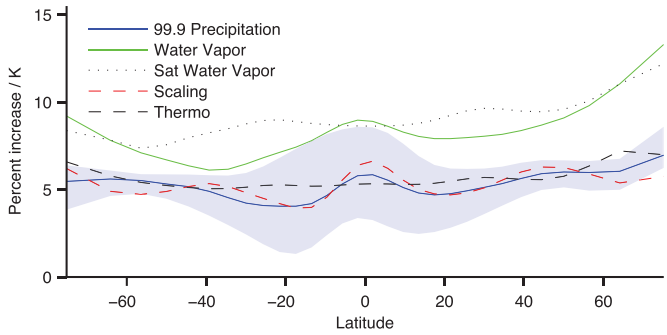

Fig. 2. Fractional changes in the 99.9th percentile of daily precipitation (blue), zonally averaged atmospheric water vapor content (green), saturation water vapor content of the troposphere (black dotted), full precipitation extremes scaling (Eq. **2**) (red dashed), and thermodynamic scaling for precipitation extremes (black dashed). The lines show multimodel medians of the fractional changes relative to 20th-century values, normalized by the global-mean change in surface air temperature for each model. Model scatter is shown for the fractional change in precipitation extremes using the interquartile range (shading). The saturation water vapor content is calculated using an average of the climatological monthly-mean temperature over all times and longitudes at which the extreme precipitation occurs.

Climatology Project (GPCP) (19) (Fig. 1). However, there are considerable uncertainties in observations of precipitation, and other studies using different datasets or different measures of precipitation extremes have found that climate models underestimate precipitation extremes relative to observations (10–12, †). The simulated precipitation extremes increase at all latitudes as the climate warms, particularly in the tropics where they are largest (Fig. 1). The water vapor content of the atmosphere also increases at all latitudes, but precipitation extremes do not scale with the water vapor content (Fig. 2). In the multimodel median, precipitation extremes increase with global-mean surface air temperature at a smaller rate than the zonal-mean atmospheric water vapor content (Fig. 2). For example, at 60°N, the 99.9th percentile of daily precipitation increases at 6% K^{-1} in the multimodel median, compared with 10% K^{-1} for the atmospheric water vapor content. (Both rates of increase are normalized by the change in global-mean surface air temperature for each model before taking the median among all models.) There is larger intermodel scatter in the tropics than in the extratropics in both the precipitation extremes and their fractional changes with warming (Figs. 1 and 2).

Precipitation extremes also do not scale with water vapor content in individual models. Extratropical precipitation extremes consistently increase less rapidly with surface air temperature than does the extratropical water vapor content (Fig. 3*A*). The rate of change in tropical precipitation extremes varies widely among models; changes in tropical precipitation extremes normalized by the increase in tropical surface air temperature range from 1.3% K^{-1} to 30% K^{-1}. (Models with small tropical increases can be more easily distinguished in Fig. S1, which is the same as Fig. 3 but with logarithmic axis scales.) In most models, tropical precipitation extremes increase less rapidly than or at a similar rate as tropical water vapor content; for two outlying models (both from GFDL), the increases in tropical precipitation extremes are much greater. The behavior of tropical precipitation extremes in the GFDL models is also sensitive to the percentile considered, with close to zero (<1% K^{-1}) changes in tropical precipitation extremes at the 99th percentile.

Precipitation extremes may occur preferentially in certain seasons or at certain longitudes. Furthermore, one may hypothesize that precipitation extremes depend on the saturation water vapor content of the atmosphere when they occur, rather than on

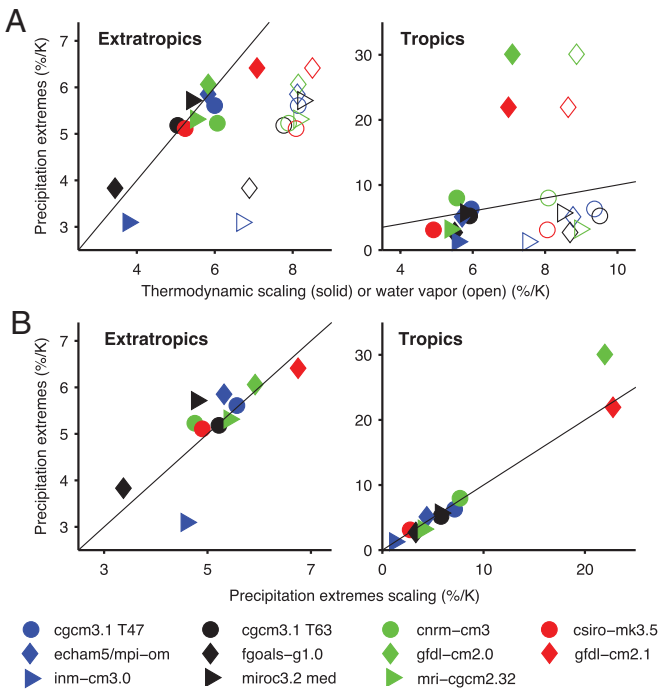

Fig. 3. Fractional changes in the 99.9th percentile of daily precipitation for each model versus changes in atmospheric water vapor content and scalings for precipitation extremes. (*A*) Atmospheric water vapor content (open symbols) and the thermodynamic scaling that neglects changes in upward velocity (solid symbols). (*B*) Full scaling for precipitation extremes. The fractional change are relative to 20th-century values, averaged over the extratropics (*Left*) or tropics (*Right*) and normalized by the change in surface air temperature averaged over the extratropics or tropics. Solid lines correspond to one-to-one relationships. The extratropics are defined as the regions poleward of 30° latitude, and the tropics are defined as the region equatorward of 30° latitude.

†Models and observations may agree more closely in our study than in some other studies in part because we use percentiles of precipitation including all days (dry and wet) and because we spatially average observations to typical model resolution. The precipitation extremes scaling discussed below implies that if models approximately reproduce the distribution of vertical velocities but inaccurately simulate the frequency of wet days, inclusion of all days in the percentile analysis will give the most favorable comparison.

the mean water vapor content, which change differently in part because the relative humidity does not stay exactly constant as the climate warms (20). Therefore, we also calculate the saturation water vapor content of the troposphere from an average of climatological monthly-mean temperatures over the longitudes and days when the extreme precipitation occurs. The conclusions are qualitatively similar, irrespective of whether changes in precipitation extremes are compared with changes in this measure of saturation water vapor content or in mean water vapor content (Fig. 2). For example, the median rate of increase in the 99.9th percentile of precipitation at 30°N and 30°S is approximately half the median rate of increase in saturation water vapor content. So precipitation extremes do not scale with the local seasonal mean saturation water vapor content of the atmosphere either.

Precipitation Extremes Scaling. The changes in precipitation extremes seen in the climate simulations can be understood by considering the dynamics and thermodynamics of precipitation events (8, 21). In such events, air rises and cools adiabatically, water vapor condenses, latent heat is released, and condensate precipitates. The condensation rate needed to maintain the water vapor content of the rising air near saturation is given by

$$c = -\omega \left. \frac{dq_s}{dp} \right|_{\theta^*}, \qquad [1]$$

where ω is the vertical velocity in pressure (p) coordinates, and the derivative of the saturation specific humidity (q_s) is taken along a moist adiabat with constant saturation equivalent potential temperature (θ^*) (8). We are assuming that diabatic processes other than latent heating are negligible when precipitation extremes occur. The condensation rate (Eq. **1**), and with it the precipitation rate, in precipitation extremes does not increase as rapidly with temperature as the saturation specific humidity because the moist-adiabatic derivative of saturation specific humidity, $dq_s/dp|_{\theta^*}$, does not increase as rapidly with temperature as the saturation specific humidity (22). For example, at a temperature of 280 K and a pressure of 800 hPa, it increases with temperature at 2.9% K^{-1}, compared with 6.9% K^{-1} for the saturation specific humidity (Fig. S2). The difference arises because the rate of decrease of temperature for rising air (the moist-adiabatic lapse rate) is smaller at higher temperatures.

Because along a moist adiabat, $dq_s \approx -(c_p/L)(T/\theta)d\theta$, with dry potential temperature θ and assuming a constant latent heat of vaporization L, the condensation rate (Eq. **1**) can alternatively be written as $c \approx \omega\, c_p T/(L\theta) d\theta/dp|_{\theta^*}$, where c_p is the heat capacity of air (22). The latent heat release in condensation balances the product of the vertical velocity and a static stability measure along a moist adiabat, that is, it balances the adiabatic cooling in updrafts. The smaller increase in precipitation extremes than in water vapor content as the climate warms can then be viewed as consequence of this static stability changing more slowly with temperature than the saturation specific humidity. An alternative derivation of the expression (Eq. **1**) for the condensation rate that is applicable to the tropics (and applies equally well to evaporation in downdrafts) follows from the Eulerian thermodynamic equation by neglecting horizontal, temporal, and radiative tendencies, and using that the static stability is approximately moist adiabatic.

Precipitation extremes depend on the temperatures at which they occur, which, in middle and high latitudes, are generally higher than the local climatological mean temperatures. For example, during the events when the 99.9th percentile of daily precipitation occurs, according to NCEP2 reanalysis temperature data (23) and GPCP precipitation data (19), extratropical temperatures at 600 hPa are up to 5 K higher than in the mean (Fig. S3).[‡] The temperatures at which extreme precipitation events occur need not increase at the same rate as the local climatological mean temperatures; for example, at latitudes where precipitation is related to poleward movement of air masses, they may be tied more closely to mean temperatures farther equatorward, and mean temperatures change differently at different latitudes in global warming simulations (25).

Taking into account these factors, we can express the intensity of precipitation extremes at a given latitude as

$$P_e \sim -\left\{ \omega_e \left. \frac{dq_s}{dp} \right|_{\theta^*, T_e} \right\}. \qquad [2]$$

Here, P_e is a high percentile of precipitation, ω_e the corresponding upward vertical velocity, $\{\cdot\}$ is a mass-weighted integral over the troposphere, and the moist-adiabatic derivative of saturation specific humidity is evaluated at the conditional mean temperature T_e when extreme precipitation occurs. A large-scale average over precipitation systems is implied, so that ω_e is a net upward velocity including the contribution of any convective downdrafts driven by reevaporation of condensate, and the net precipitation rate P_e appears on the left-hand side rather than a column-integrated condensation rate. A similar scaling agrees with the behavior of precipitation extremes in simulations of a wide range of climates with an idealized general circulation model (8). We evaluate the temperature T_e and upward velocity ω_e as an average over all days and longitudes at which extreme precipitation occurs,[§] using the vertical velocity ω resolved on the models' grid, not including a subgrid component. The scaling (Eq. **2**) captures the behavior of the precipitation extremes at all latitudes in the multimodel median of the global warming simulations (Fig. 2), and in the simulations individually, except for one outlier (Fig. 3*B*).

The precipitation extremes scaling can be simplified under certain conditions, so that precipitation extremes scale with the mean moisture convergence at the base of storms, as suggested in ref. 7. If the thermal structure of the atmosphere is moist adiabatic on large scales when precipitation extremes occur, and if the vertical structure of the vertical velocity is neglected, then the precipitation extremes scaling can be directly integrated in the vertical, with the result that it behaves like the low-level saturation specific humidity multiplied by a measure of the vertical velocity or low-level mass convergence (8). There is no a priori justification for neglecting the vertical structure of the vertical velocity, but once this assumption is made and the vertical integral is performed, the boundary term at the tropopause is negligible. In the extratropics, the atmosphere can be more stable than moist adiabatic, and so the precipitation extremes scaling cannot be generally simplified in this way, except in the case of sufficiently deep vertical or slantwise moist convection. Nevertheless, for the climate change simulations considered here, the changes in the thermodynamic precipitation extremes scaling are similar to the changes in saturation specific humidity evaluated using the lowest-level temperature when precipitation extremes occur (Fig. S4). If a higher level is used (e.g., at the top of the boundary layer), the agreement is worse. In the tropics, the low-level saturation specific humidity increases more slowly with temperature than the atmospheric

[‡]Analysis of the covariability of monthly mean precipitation and surface temperature also reveals a positive correlation between temperature anomalies and precipitation at high latitudes in winter, but different correlations in other seasons and regions (24); these results are not directly comparable with our study because we use daily data and extremes of precipitation.

[§]The scaling used here is more general than that used in ref. 8, where it was assumed that the extreme upward velocity scales with the root-mean-square vertical velocity.

water vapor content because the increases in temperature are greater aloft (25), and so we again reach the conclusion that if upward velocities do not change, precipitation extremes increase more slowly with surface temperature than the water vapor content. This simplified version of the precipitation extremes scaling may be useful when there is limited data available for the evaluation of scalings; it implies that the amount of near-surface water vapor is more relevant to precipitation extremes than the total column water vapor.

Contributions to Changes in Precipitation Extremes. Changes in upward velocities associated with tropical precipitation extremes are not consistent among models. To illustrate this, we also consider a purely thermodynamic scaling, calculated by omitting ω_e from the expression (Eq. **2**). We obtained similar results when the upward velocity ω_e is retained in the scaling but is not allowed to change with climate, such that the vertical structure of the upward velocity is taken into account. The full precipitation extremes scaling is adequate for all models (except for one outlier) in the extratropics and tropics (Fig. 3*B*), whereas the thermodynamic scaling only gives good agreement in the extratropics (Fig. 3*A*). Thus, the large intermodel scatter in the changes in tropical precipitation extremes is caused by widely varying (positive and negative) changes in the upward velocity. This discrepancy likely arises because different climate models use different parameterizations of moist convection (9).

In addition to changes in upward velocity, precipitation extremes do not scale with water vapor content because of changes in the moist-adiabatic lapse rate and the temperature anomaly when precipitation extremes occur. We evaluated the relative contributions of all these factors to the precipitation extremes scaling by comparing changes in the full scaling with changes in modified scalings (Fig. S5). The relative contributions are given as differences between the modified and unmodified scalings, for the multimodel medians of fractional changes in each scaling normalized by the changes in global-mean surface air temperature. Changes in the moist-adiabatic lapse rate are important at all latitudes (global-mean contribution $-3.4\%\ \mathrm{K}^{-1}$) but have greatest effect at low latitudes. The modified scaling in this case was calculated by replacing the moist-adiabatic derivative of saturation specific humidity with the dry-adiabatic derivative of saturation specific humidity (8). The effect of changes in the temperature anomaly when precipitation extremes occur is relatively small, with a global-mean contribution of $-0.5\%\ \mathrm{K}^{-1}$; they have a larger effect in different seasons at high latitudes. The modified scaling in this case was calculated using an average of climatological monthly mean temperatures over the longitudes and days when the extreme precipitation occurs. Changes in upward velocity have a global-mean contribution of $-0.3\%\ \mathrm{K}^{-1}$, but in the tropics, they do not change consistently among models. The modified scaling in this case was the thermodynamic scaling discussed above. Our analysis suggests that changes in the moist-adiabatic lapse rate are the primary moderating influence on precipitation extremes, at least in the extratropics where changes in upward velocities are consistent among models.

Generality of Results. Similar conclusions can be drawn for changes in precipitation extremes in individual seasons and over land or ocean separately (Figs. S6 and S7). Likewise, the 99th and 99.99th percentiles of daily precipitation in the extratropics increase at similar rates as the 99.9th percentile; however, they differ in the tropics (Fig. S8). Consistent with previous studies, we find that there is a negative dynamical contribution to the change in tropical precipitation extremes at the 99th percentile (26, 27). Because the full precipitation extremes scaling is accurate for each percentile considered, and the fractional changes in the thermodynamic scaling do not vary strongly with percentile, the differences in the fractional increases in precipitation extremes at different percentiles in the tropics arise because of differences in the changes in upward velocities.

Conclusions

We have given a physical basis for how precipitation extremes change as the climate warms in a range of climate model simulations, and we successfully used a general scaling to relate quantitative changes in precipitation extremes to changes in temperature and vertical velocity. In the extratropics, in agreement with the theory, climate models consistently predict that precipitation extremes increase more slowly with surface air temperature than atmospheric water vapor content. In the tropics, most climate models also predict that precipitation extremes increase more slowly than atmospheric water vapor content. However, we have shown that the tropical changes are not consistent among models because of widely varying changes in upward velocities associated with precipitation extremes. The analysis of simulations has shown that precipitation extremes scale more similarly to near-surface water vapor concentrations than to total atmospheric water vapor content. However, this empirical result depends on where near the surface the water vapor concentration is evaluated. The precipitation extremes scaling used here is more easily justifiable on physical grounds, makes minimal assumptions about the character of extreme precipitation events, and should be more generally applicable.

Our results imply that current climate models cannot reliably predict changes in tropical precipitation extremes, despite the consistency in magnitude that we find between precipitation extremes from one observational dataset and the multimodel median. The inaccurate simulation of the upward velocities may explain not only the intermodel scatter in changes in tropical precipitation extremes but also the inability of models to reproduce observed interannual variability (10). In the extratropics, in contrast, the upward velocity appears to be controlled to a greater extent by large-scale processes (synoptic eddies), so that the changes in precipitation extremes are less dependent on details of convection parameterizations. To improve predictions of tropical precipitation extremes, it is essential to constrain changes in the upward velocity associated with precipitation extremes.

Methods

Model and Observational Data. We used as wide a range of climate models as possible from CMIP3, given constraints on data availability and inconsistencies in the data from some climate models. The CMIP3 identifiers of the models used are as follows: cgcm3.1 (T47), cgcm3.1 (T63), cnrm-cm3, csiro-mk3.5, echam5/mpi-om, fgoals-g1.0, gfdl-cm2.0, gfdl-cm2.1, inm-cm3.0, miroc3.2 (medres), and mri-cgcm2.32. The time periods used were 1981–2000 and 2081–2100, with the exception of the fgoals-g1.0 model for which 1981–1999 and 2081–2099 were used. The precipitation extremes (or their fractional changes) for each model are evaluated on the native model grids, and are then interpolated to a 30-point equal-area latitude grid before multimodel medians are taken.

The observational values for precipitation extremes in Fig. 1 are derived from daily precipitation data at horizontal resolution 1° from the Global Precipitation Climatology Project (GPCP) for the period 1997–2006 (19). We regridded the GPCP data to a 3° grid by averaging over the 9 closest neighbors at each grid point because the climate models have an effective horizontal resolution of 2°-3° or coarser, and because the magnitude of extremes at a given percentile depends on horizontal resolution (28). This degradation of the resolution of the GPCP data is consistent with the spatial averaging approach that has been advocated for the comparison of precipitation extremes at different resolutions (28). The global-mean of the 99.9th percentile of daily precipitation shown in Fig. 1 increases from 44.5 $\mathrm{mm\cdot day}^{-1}$ to 51.4 $\mathrm{mm\cdot day}^{-1}$ if the original 1° data are used in the analysis. The fact that spatial resolution affects the absolute value of precipitation extremes does not directly affect the main results of our article, which involve fractional changes in precipitation extremes.

Evaluation of Scaling and Saturation Water Vapor Content. The precipitation extremes scaling was evaluated using mean values of the daily temperature and daily upward velocity at each pressure level conditioned on extreme (surface) precipitation occurring. To reduce noise, the conditional mean of the temperature T_e and the upward velocity ω_e for a given percentile of precipitation was taken over all days and longitudes for which the precipitation lies in a finite range, chosen for the nth percentile as the range between the $100 - (3/2)(100 - n)$ and $100 - (1/2)(100 - n)$ percentiles (8). The temperature T_e differs from the temperature used to calculate the saturation water vapor content in Fig. 2 because it includes the temperature anomaly due to synoptic variability.

In evaluating the precipitation extremes scaling and the saturation water vapor content of the troposphere, vertical pressure integrals were performed up to the highest available pressure level or the tropopause, whichever was lower. The tropopause was defined as the highest level with a temperature lapse rate of 2 K·km^{-1} (the highest level available in any model used is 10 hPa for the daily temperature data). The moist-adiabatic lapse rate used to evaluate $dq_s/dp|_{\theta^*,Te}$ in the precipitation extremes scaling was calculated based on pseudoadiabatic ascent. The saturation vapor pressure was evaluated according to a modified Tetens formula (29), as the saturation vapor pressure over ice for temperatures below −23 °C, the saturation vapor pressure over liquid water above 0 °C, and a quadratic interpolation between the two at intermediate temperatures.The vertical (pressure) velocity ω was calculated using the continuity equation and daily horizontal winds and surface pressure. The accuracy of this calculation is limited by the vertical resolution of the model data available (which was itself vertically interpolated from higher-resolution model output). For latitudes poleward of 60°, ω was assumed to be zero at the highest pressure level and the continuity equation was integrated downwards. This procedure does not require evaluation of the near-surface ω as a boundary condition, but it is not appropriate at lower latitudes, where the tropopause is often higher than the highest available pressure level (200 hPa in many cases). Instead, for latitudes equatorward of 60°, the near surface ω was estimated using surface pressure data and low-level winds, and the continuity equation was integrated upwards. In the calculation of the conditional-mean upward velocity ω_e, the velocity ω is set to zero if it is directed downward.

The changes in the saturation water vapor content of the troposphere in Fig. 2 were calculated based on an average of the climatological monthly-mean temperature over all days and longitudes for which the precipitation was in the percentile range used to define T_e and ω_e. The temperature so defined allows a direct comparison at each latitude between the changes in the mean saturation water vapor content of the troposphere at the longitudes and months when the precipitation extremes occur and the changes in the precipitation extremes scaling. The climatological monthly-mean temperature for a given location and month was defined as the mean temperature for that month averaged over the 20-year period in question.

ACKNOWLEDGMENTS. We thank the modeling groups, the Program for Climate Model Diagnosis and Intercomparison and the World Climate Research Programme's Working Group on Coupled Modelling for their roles in making available the World Climate Research Program Coupled Model Intercomparison Project phase 3 multimodel dataset. Support of this dataset was provided by the Office of Science, U.S. Department of Energy. This work was supported by David and Lucile Packard Fellowship and by the National Science Foundation Grant ATM-0450059. The Global Precipitation Climatology Project 1-degree daily precipitation dataset was downloaded from http://www1.ncdc.noaa.gov. National Centers for Environmental Prediction-Department of Energy Reanalysis 2 data were provided by the National Oceanic and Atmospheric Administration/Office of Oceanic and Atmospheric Research/Earth System Research Laboratory Physical Sciences Division at www.cdc.noaa.gov.

1. Held IM, Soden BJ (2006) Robust responses of the hydrological cycle to global warming. *J Climate* 19:5686–5699.
2. Kharin VV, Zwiers FW, Zhang X, Hegerl GC (2007) Changes in temperature and precipitation extremes in the IPCC ensemble of global coupled model simulations. *J Climate* 20:1419–1444.
3. Sun Y, Solomon S, Dai A, Portmann RW (2007) How often will it rain? *J Climate* 20:4801–4818.
4. Parry ML, et al. (2007) in *Climate Change 2007: Impacts, Adaptation and Vulnerability* (Cambridge Univ Press, Cambridge, UK), pp 23–78.
5. Allen MR, Ingram WJ (2002) Constraints on future changes in climate and the hydrologic cycle. *Nature* 419:224–232.
6. Pall P, Allen MR, Stone DA (2007) Testing the Clausius-Clapeyron constraint on changes in extreme precipitation under CO2 warming. *Clim Dyn* 28:351–363.
7. Trenberth KE (1999) Conceptual framework for changes of extremes of the hydrological cycle with climate change. *Clim Change* 42:327–339.
8. O'Gorman PA, Schneider T (2009) Scaling of precipitation extremes over a wide range of climates simulated with an idealized GCM. *J Climate*, in press.
9. Wilcox EM, Donner LJ (2007) The frequency of extreme rain events in satellite rain-rate estimates and an atmospheric general circulation model. *J Climate* 20:53–69.
10. Allan RP, Soden BJ (2008) Atmospheric warming and the amplification of precipitation extremes. *Science* 321:1481–1484.
11. Dai A (2006) Precipitation characteristics in eighteen coupled climate models. *J Climate* 19:4605–4630.
12. Sun Y, Solomon S, Dai A, Portmann RW (2006) How often does it rain? *J Climate* 19:916–934.
13. Easterling DR, et al. (2000) Observed variability and trends in extreme climate events: A brief review. *Bull Amer Meteor Soc* 81:417–425.
14. Frich P, et al. (2002) Observed coherent changes in climatic extremes during the second half of the twentieth century. *Clim Res* 19:193–212.
15. Groisman PY, et al. (2005) Trends in intense precipitation in the climate record. *J Climate* 18:1326–1350.
16. Lenderink G, van Meijgaard E (2008) Increase in hourly precipitation extremes beyond expectations from temperature changes. *Nat Geosci* 1:511–514.
17. Changnon SA, Kunkel KE (1995) Climate-related fluctuations in midwestern floods during 1921–1985. *J Water Resour Planning Manage* 121:326–334.
18. Kunkel KE, Andsager K, Easterling DR (1999) Long-term trends in extreme precipitation events over the conterminous United States and Canada. *J Climate* 12:2515–2527.
19. Huffman GJ, et al. (2001) Global precipitation at one-degree daily resolution from multisatellite observations. *J Hydrometeor* 2:36–50.
20. Lorenz DJ, DeWeaver ET (2007) The response of the extratropical hydrological cycle to global warming. *J Climate* 20:3470–3484.
21. Iribarne JV, Godson WL (1981) *Atmospheric Thermodynamics (Section 9.14), Geophysics and Astrophysics Monographs* (D. Reidel, Dordrecht, The Netherlands), 2nd Ed, p 259.
22. Betts, A, Harshvardhan K (1987) Thermodynamic constraint on the cloud liquid water feedback in climate models. *J Geophys Res* 92:8483–8485.
23. Kanamitsu M, et al. (2002) NCEP-DOE AMIP-II Reanalysis (R-2), *Bull Amer Meteor Soc* 83:1631–1643.
24. Trenberth KE, Shea DJ (2005) Relationships between precipitation and surface temperature. *Geophys Res Lett* 32:L14703.
25. Meehl GA, et al. (2007) *Climate Change 2007: The Physical Science Basis* (Cambridge Univ Press, Cambridge, UK), Ch 10, pp 747–846.
26. Emori, S and Brown, S. J (2005) Dynamic and thermodynamic changes in mean and extreme precipitation under changed climate. *Geophys Rev Lett* 32:L17706.
27. Gastineau G, Soden BJ (2009) Model projected changes of extreme wind events in response to global warming, *Geophys Rev Lett* 36:L10810.
28. Chen CT, Knutson T (2008) On the verification and comparison of extreme rainfall indices from climate models. *J Climate* 21:1605–1621.
29. Simmons AJ, Untch A, Jakob C, Kållberg P, Undén P (1999) Stratospheric water vapour and tropical tropopause temperatures in ECMWF analyses and multi-year simulations. *Quart J Roy Meteor Soc* 125:353–386.